Bone Marrow Cavity Segmentation using Graph-cuts with Wavelet-Based Texture Feature

Article *in* Journal of Bioinformatics and Computational Biology · August 2017

DOI: 10.1142/S0219720017400042

7 authors, including:

Tomohiro Mashita
Osaka University
52 PUBLICATIONS **172** CITATIONS
SEE PROFILE

Shigeto Seno
Osaka University
72 PUBLICATIONS **2,479** CITATIONS
SEE PROFILE

Haruo Takemura
Osaka University
306 PUBLICATIONS **3,325** CITATIONS
SEE PROFILE

Hideo Matsuda
Osaka University
188 PUBLICATIONS **7,720** CITATIONS
SEE PROFILE

Journal of Bioinformatics and Computational Biology
Vol. 15, No. 5 (2017) 1740004 (16 pages)

DOI: 10.1142/S0219720017400042

Bone marrow cavity segmentation using graph-cuts with wavelet-based texture feature

Hironori Shigeta[*,§], Tomohiro Mashita[*,†], Junichi Kikuta[‡], Shigeto Seno[*], Haruo Takemura[*,†], Masaru Ishii[‡] and Hideo Matsuda[*]

[*]*Graduate School of Information Science and Technology, Osaka University Yamadaoka 1-5, Suita, Osaka, Japan*

[†]*Cybermedia Center, Osaka University, Japan*

[‡]*Graduate School of Medicine and Frontier Biosciences Osaka University, Japan*

[§]*shigeta@ist.osaka-u.ac.jp*

Received 23 August 2017
Accepted 23 August 2017
Published 7 September 2017

Emerging bioimaging technologies enable us to capture various dynamic cellular activities *in vivo*. As large amounts of data are obtained these days and it is becoming unrealistic to manually process massive number of images, automatic analysis methods are required. One of the issues for automatic image segmentation is that image-taking conditions are variable. Thus, commonly, many manual inputs are required according to each image. In this paper, we propose a bone marrow cavity (BMC) segmentation method for bone images as BMC is considered to be related to the mechanism of bone remodeling, osteoporosis, and so on. To reduce manual inputs to segment BMC, we classified the texture pattern using wavelet transformation and support vector machine. We also integrated the result of texture pattern classification into the graph-cuts-based image segmentation method because texture analysis does not consider spatial continuity. Our method is applicable to a particular frame in an image sequence in which the condition of fluorescent material is variable. In the experiment, we evaluated our method with nine types of mother wavelets and several sets of scale parameters. The proposed method with graph-cuts and texture pattern classification performs well without manual inputs by a user.

Keywords: Image segmentation; fluorescence microscopy images; wavelet texture analysis.

1. Introduction

Advance in bioimaging technologies such as microscopic imaging techniques has made it possible to capture various dynamic cellular activities *in vivo*. These technologies are expected to contribute to the discovery of new drugs and will clarify

the mechanisms of disease. Multiphoton excitation microscopy is one of the new imaging technologies that can observe deeply the cellular activities in living tissues *in vivo*. It was previously difficult to observe bone marrow *in vivo* because it resides inside of hard bones which mainly consist of calcium. Multiphoton excitation microscopy enabled observation images inside bone marrow *in vivo*, such as blood flow and cellular activities. Kikuta *et al.* utilized intravital multiphoton microscopy to observe osteoclast resorption and differentiate between static-resorptive (R) osteoclasts and moving-nonresorptive (N) osteoclasts.[1]

In order to reveal cellular activities in images of specific tissues, specific cellular activities or regions must be accurately detected from among a large number of image sequences. In some cases, image sequences to be searched are four-dimensional and the resolution of microscopes are improved day by day. That is, the size of the bioimage data is too large for manual analysis such as detecting a particular cellular activity. Therefore, it is necessary to be able to detect specific regions or cellular activities within the large image data. Since many phenomena related to the mechanism of bone remodeling and osteoporosis are observed in bone marrow cavity (BMC), it is required to automatically segment BMC regions from bone images.

However, there are several issues in BMC segmentation because these images contain ambiguities due to overlapping of the BMC, blood flow, cells, bone, and other tissues. Furthermore, in some types of image sequences, the intensity of the BMC regions varies due to seeping of fluorescent material. We have been working on automatic segmentation of BMC.[2–4] Although our previous methods produce good results, manual inputs by a user are required such as clicking or drawing some positions of the foreground (BMCs) and background (not BMCs) pixels for each image or dataset.

As it is assumed that data will increase rapidly, it is becoming important to perform automatic analysis at once for a large amount of data and to discover new biological knowledge by statistical analysis. Another importance of automatic analysis is that it enables bias-free evaluation. When analyzing images manually, a bias is generated when selecting the regions, which might lead to different conclusions for each researcher. The reproducibility is guaranteed with the automatic analysis, which enables objective discussion on the data. To reduce manual inputs and to achieve automatic segmentation, we propose a method for detecting BMC regions by texture analysis with wavelet transformation (WT) and classifying by using support vector machine (SVM). Furthermore, since the output of texture analysis does not consider spatial continuity, we also apply graph-cuts for image segmentation with the results of wavelet analysis.

2. Related Works

Bioimaging technologies generate massive and a wide variety of bioimages. Based on such technologies, many bioimage processing methods have been studied. Cell tracking is one of the main problems in bioimage processing. Fujisaki *et al.* proposed a method to detect and track protein molecules.[5] Meijering *et al.* surveyed several

methods of cell tracking, and one of their conclusions indicates that there is no universal solution for tracking problems in cell and developmental biology.[6] In bioimage tracking, there are some special events including cell fusion, cell division, cell death, and so on. Liu *et al.* proposed a method to detect and track such events.[7] The studies of Olivieri *et al.* analyzed images taken with multiphoton excitation microscopy.[8] They proposed a cell tracking method and a tool for live cell images of lymphocytes. Since each bioimage has its unique attributes, suitable image analysis methods tend to be combined. For example, graph-cuts and wavelet are combined to segment retinal layers[9] or choroid layers.[10] However, it is not applicable to BMC segmentation because these methods are specialized in their target images and the way of combination is also adjusted according to target attributes.

In addition to the studies focusing on cell appearance or behavior in images, there are also studies focusing on the imaging process of a microscope. Yin *et al.* modeled imaging with phase contrast microscopy.[11] In their study, they modeled characteristics of microscopy and simplified captured images. As a result, the images were simplified and the cells were easily segmented by simple thresholding. As mentioned above, there is no universal solution for analyzing bioimages due to the diversity of the characteristics of the microscope and the variety of target cells. The *in vivo* images inside the bone tissue captured by multiphoton excitation microscopy are one such type of bioimages.

3. BMC Segmentation

Figure 1 shows an example of BMC image including bone, blood vessels, BMCs, and so on. This image was taken by multiphoton excitation microscopy. In the experiment, the mouse is injected with fluorescein isothiocyanate (FITC) into the blood vessels in the skull bone tissue. FITC is shown as the green channel in Fig. 1, mainly flowing through blood vessels. However, as shown in Fig. 2, FITC seeps into bone marrow areas with time. As a result of seeping, the intensity in BMC regions increases over time. Although a simple image segmentation based on intensity performs well in early frames, it is basically unavailable after seeping because the intensity in bone marrow regions gets closer to the blood vessels' level. Ideally,

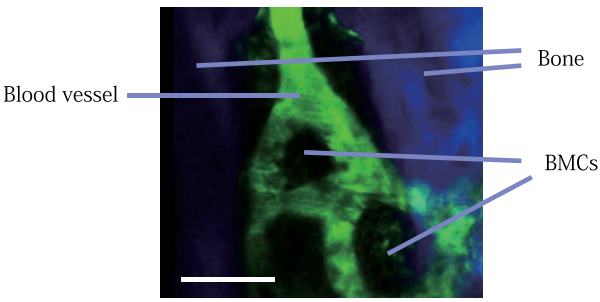

Fig. 1. Example of BMC image. (scale bar: 50 μm).

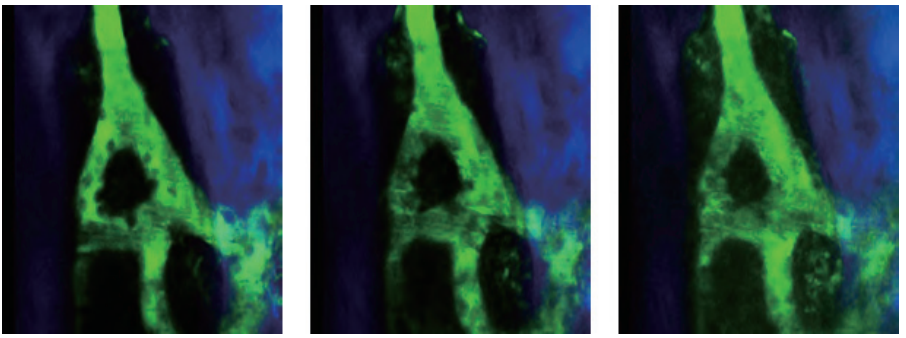

Fig. 2. Temporal variation of images: time advances from left to right.

segmentation under particular seeping conditions should be achieved so that observations may be made multiple times for a mouse. Therefore, a more robust segmentation method is required than the intensity-based method. As shown in Fig. 2, the intensity in the BMC region is high but heterogeneous, and there is a pattern different from the pattern of the blood vessel region. This kind of BMC pattern commonly appears in other BMC images. We therefore propose a method to analyze texture pattern analysis using WT. The result of texture analysis is classified by SVM to judge the area. This approach makes it possible to classify arbitrary pixels in an arbitrary frame. However, as spatial continuity is not taken into consideration, we integrated the result of texture pattern classification into graph-cuts-based segmentation method, commonly used for image segmentation. The overview of our system is shown in Fig. 3.

3.1. *Wavelet transformation*

Two-dimensional continuous WT for a function $f(x)$ is defined by the following equations:

$$T_f(a,b,\theta) = \int_{\mathcal{R}^2} f(x)\frac{1}{a}\bar{\psi}\left(r_{-\theta}\left(\frac{x-b}{a}\right)\right)dx, \tag{1}$$

$$r_\theta = \begin{pmatrix} \cos(\theta) & -\sin(\theta) \\ \sin(\theta) & \cos(\theta) \end{pmatrix}, \quad \theta \in [0, 2\pi), \tag{2}$$

where ψ, $a(a \in \mathcal{R}^+)$, and $b(b \in \mathcal{R}^2)$ means mother wavelet, scale parameter, and shift parameter, respectively, and $\bar{\psi}$ denotes the complex conjugate of ψ. Since scale parameter a has the effect to stretch the function, it is possible to correspond to various frequency of signals. Shift parameter b virtually represents coordinates in two-dimensional WT. θ represents the direction to apply WT. r_θ has the function to rotate input signals. There are two types of WT, continuous and non-continuous. We use continuous WT because it is suitable for describing image features. To save processing time, we employ fast WT. As the scale parameter a is fixed in fast WT, the wavelet function in Eq. (1) becomes a convolution form of input signal and mother

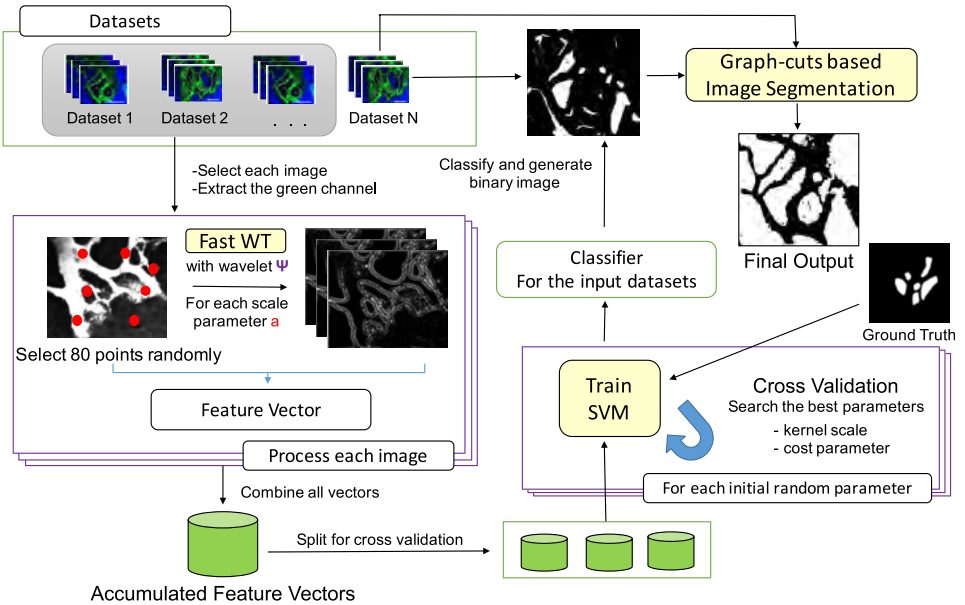

Fig. 3. Overview of our method.

wavelet, which enables fast calculation by Fourier transform. Although the continuity regarding the scale parameter a is unavailable, we apply multiple scale parameters as an approximation of continuous scale parameter.

3.2. *BMC classification*

In the proposed method, absolute values of wavelet coefficients are used for the feature values. Since the scale parameter a is constant in fast WT, we provide several scale parameters. Although WT has directional parameter θ, the feature value should be independent from the directional variation of input image. To ignore the directional variation, it is suitable to use isotropic wavelets. However, also to examine results of anisotropic wavelets, the summation of all directions is used as the feature value at each wavelet equally. Eventually, the dimension of a feature vector of each pixel (represented by b) is the same as the element count of a chosen scale parameter set. Because the magnification ratio of an input image depends on the dataset, the scale parameter a should be normalized along with that. Therefore, a is defined as $a = a_b \cdot P_D$, where a_b denotes the base scale parameter and P_D is the scale factor and defined as the number of pixels in 50 μm. Since the BMCs appear only in the blood channel, the green channel is used.

There are many types of mother wavelet applicable for our method. As mentioned above, it is also necessary to provide a set of several scale parameters. Eventually, mother wavelet ψ and sets of base scale parameters a_b should be evaluated. In order to classify the BMCs using WT, our method generates a texture feature vector array

and classify vector arrays. When classifying textures using SVM, it is also necessary to optimize two SVM parameters: kernel scale and cost parameters. Since the classification performance for each parameter can be evaluated by cross-validation loss with ground truth data, our method searches for better classification parameters. Manually segmented images for each dataset are prepared as ground truth data. Given the mother wavelet ψ and sets of base scale parameters a_b, we apply the following procedure to obtain theSVM classifier for the input datasets:

(1) Generating a texture feature vector array.
   - Apply WT with the mother wavelet ψ and the set of scale parameters a to each image.
   - Choose sample points and calculate feature vectors from WT results.
     — Although more sample points are better, we choose 80 sample points randomly from each image of every dataset because of computational limitation.
   - Create one feature vector array by accumulating feature vectors of all images.

(2) Optimize the parameters for SVM. (Generate random initial parameters and search local minimum nearby.)
   - Partition the texture feature vector array for k-fold cross-validation.
   - Randomly generate initial values for each parameter: the kernel scale and the cost parameter.
     — More trials are better to get appropriate parameters while computational costs increase more. Therefore, 15 initial values are chosen respectively considering computational complexity.
   - For each initial parameter set,
     — Conduct k-fold cross-validation with the initial parameter set and calculate cross-validation loss using ground truth images.
     — Find local minimum loss nearby the initial parameter set by the Nelder–Mead simplex method.[12]
     — Output the loss value.
   - Select a parameter set with the smallest loss value from the 15 optimized parameter sets. (The best parameters set is chosen.)

(3) Train the classifier again using the all texture feature vector array with the selected parameter set.

(4) Output the SVM classifier.

3.3. *Segmentation*

Graph-cuts consist of an energy minimization algorithm widely used in low-level image processing, typified by image binarization. An energy function $E(X)$ with

label $L = \{0, 1\}$ (0 for background, 1 for foreground) and a set of pixels V is defined as follows:

$$E(X) = \sum_{v \in V} g_v(X_v) + \sum_{(u,v) \in E} h_{uv}(X_u, X_v), \tag{3}$$

where X_v is the label assigned to v, $E \subset V \times V$ is the set of interacting pairs of pixels, and $(u, v) \in E$ are adjacent pixels. In case of an image binarization problem, the function g_v is defined as the likelihood of foreground and background, and h_{uv} is defined as a smoothness function. Therefore, the term including g_v is called the data term and the term including h_{uv} is called the smoothness term. The labels that minimize the energy function are obtained by solving as a max-flow min-cut algorithm.

In commonly used graph-cuts methods as typified by Boykov's graph cuts,[13,14] the data term is basically defined only by intensity. However, as mentioned above, an intensity-based data term cannot segment the target images due to seeping of FITC, overlapping of other tissues, and others. In the proposed method, we utilized the above-mentioned SVM classifier from WT. It classifies the input image and generates a binary image. This binary image is used as input of the graph-cuts to segment the entire image. Also, since the BMCs appear only in the blood channel, the green channel is used. We apply the following equation as the data term:

$$g_v(X_v = 0) = e^{\frac{-{I_v}^2}{2\rho^2}} + \lambda g_c(v), \tag{4}$$

$$g_v(X_v = 1) = e^{\frac{-(1-I_v)^2}{2\rho^2}} + \lambda(1 - g_c(v)), \tag{5}$$

$$g_c(v) = \begin{cases} 1, & \text{BMC}, \\ 0, & \text{otherwise}, \end{cases}$$

where I_v is intensity of pixel v in the green channel that is defined as $0 \leq I_v \leq 1$, g_c is the result of classification by the SVM, λ is a weight parameter for the result of texture pattern classification, and ρ is a constant value to choose suitable to the input images.

We applied the smoothness term used in Boykov's graph-cuts:

$$h_{uv}(X_u, X_v) = \begin{cases} 0, & (X_u = X_v), \\ c \cdot e^{-\frac{(I_u - I_v)^2}{2\sigma^2}}, & (X_u \neq X_v), \end{cases} \tag{6}$$

where u is located next to v, c is a constant weight for the smooth term against the data term, and σ is also a constant, which controls the influence of intensity differences of two adjacent pixels. The parameters c, σ are manually chosen respectively.

4. Experiment

The target fluorescent material is shown in the green channel. We extracted the green channel and processed the images as gray scale images. The variation of θ in

WT is defined as every $\pi/4$, and the sum of them is used as a feature value. Regarding SVM, we applied RBF kernel, and the number of partitions for the k-fold cross-validation is 15. The error function for the cross-validation is the number of incorrect classifications. We used MATLAB R2017a with Image Processing Toolbox, Statistics Toolbox, and Wavelet Toolbox for the implementation. We also utilized maxflow 3.01 by Boykov *et al.*[15] for graph-cuts. Maxflow is written in C language and is used by MATLAB mex indirectly.

In the experiment, we used four sets of image sequences, each with its own image size, number of frames, and magnification ratio. Figure 4 shows the first frame of each image sequence and the BMC regions, which are manually segmented by a specialist. The resolution of the images, the number of frames, and the number of BMC regions are shown in Table 1. Due to the mouse's pulsing motion and others, the target image sequences need to be aligned with the first frame. To align the image sequences, we used ImageJ[16] plug ins, Turboreg[17] and Stackreg.[18]

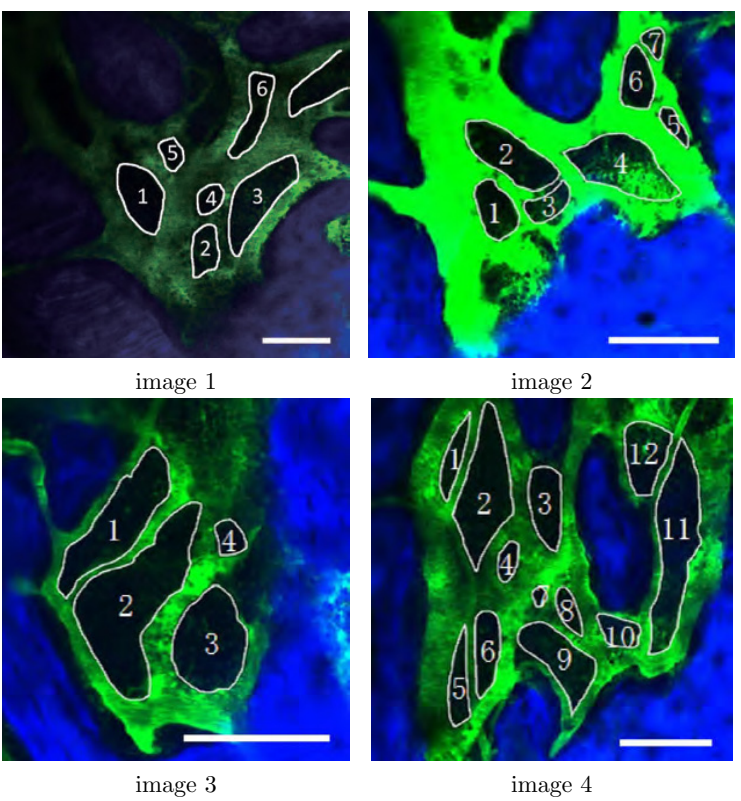

Fig. 4. Images used for the evaluation: all scale bars are 100 μm. The BMCs manually segmented by a specialist are circumscribed by white line. These regions are used for supervised data and ground truth. The green channel shows fluorescence of injected FITC and the blue channel shows bone.

Table 1. Details of BMC image used for the experiment.

	Resolution	No. of frames	No. of BMC region
Image #1	752×752	7	6
Image #2	1059×1000	15	6
Image #3	958×1000	22	4
Image #4	1001×1000	13	12

4.1. *Wavelet selection*

In order to obtain better classification, we evaluated the nine types of mother wavelets and sets of several base scale parameters. Cross-validation among datasets is conducted for the experiments: three datasets are used for the SVM training datasets, and the remaining one dataset is for testing. All the values shown in Tables 2 and 3 are the average of each combination.

Table 2 shows the results when the set of base scale parameter a_b is $\{2, 4, 16, 32, 64\}$. The examples of classifying test datasets for each wavelet are shown in Fig. 5. These results indicate that the performance of our method is highly dependent on the type of mother wavelet, and the Sinc wavelet performs better than

Table 2. Comparison among nine types of mother wavelets when the set of base scale parameter a_b is $\{2, 4, 16, 32, 64\}$: Gaussian 1, 2, and 3 mean order of derivative in Gaussian wavelet.

Mother wavelet	Precision	Recall	F-measure
Cauchy	0.047	0.005	0.009
DOG	0.417	0.074	0.126
Gaussian 1	0.308	0.058	0.097
Gaussian 2	0.314	0.068	0.112
Gaussian 3	0.314	0.068	0.112
Mexican hat	0.236	0.033	0.058
Morlet	0.154	0.026	0.044
Paul	0.094	0.012	0.028
Sinc	0.650	0.266	0.378

Table 3. Comparison among combinations of base scale parameters when the mother wavelet $\psi = \text{Sinc}$.

Combination of scales	Precision	Recall	F-measure
1, 5, 10	0.343	0.046	0.081
2, 10	0.290	0.037	0.066
10, 40	0	0	—
1, 2, 4, 8, 16	0.191	0.028	0.049
2, 4, 8, 16, 32	0.313	0.093	0.144
1, 5, 10, 40	0.271	0.050	0.084
2, 4, 16, 32, 64	0.650	0.266	0.378
2, 4, 8, 16, 32, 64	0.602	0.261	0.364

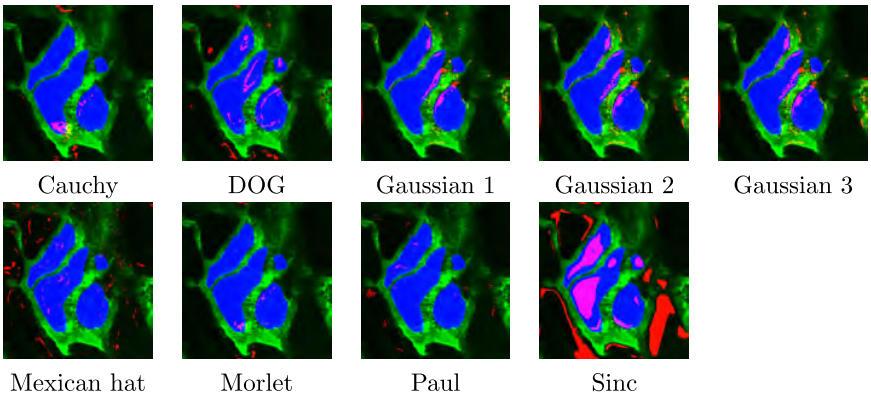

Fig. 5. Example of classification: The original image is shown in Fig. 4 (Image 3). Red channel means BMC region classified by SVM, blue channel shows region classified by a specialist (ground truth), and green channel is the same as the original image. Thus, magenta pixels are true positive, red pixels are false positive, and blue pixels are false negative.

others. While it is considered that there is generally no big difference in mother wavelet selection, the mother wavelet reflects the type of features of the input signals.[19] As other wavelets do not perform well, we consider that the response of the Sinc WT matches well with the texture pattern of the images taken by the multiphoton excitation microscopy. The Fourier transform of a/the Sinc wavelet is as follows:

$$\hat{\psi}(\omega_x, \omega_y) = [\mathrm{sinc}(A_x(\omega_x - \omega_{0x}))\mathrm{sinc}(A_y(\omega_y - \omega_{0y}))]^p, \tag{7}$$

where (ω_x, ω_y) is angular frequency defined from a and $A_x, A_y, \omega_{0x}, \omega_{0y} (\in \mathbb{R})$ are given and defined as $A_x = A_y = p = 1, \omega_{0x} = \omega_{0y} = 0$.

We evaluated the combination of base scale parameter sets as mentioned in Sec. 3.2. Table 3 shows a comparison among the combinations of base scale parameters when the mother wavelet $\psi = \mathrm{Sinc}$. This result demonstrates that the set of $\{2, 4, 16, 32, 64\}$ is better than the other combinations.

The other results of SVM with Sinc wavelet and a set of base scale parameters $\{2, 4, 16, 32, 64\}$ are shown in the second column in Fig. 6. Ground truth for comparison is also shown in Fig. 4. From these results, the pixels classified as BMC regions are essentially correct, and the blood vessel regions are also correctly classified. However, in some datasets, there are some false negative pixels.

As wavelet analysis just shows the likelihood of BMC for each pixel in terms of the texture, it can only provide limited information. Although recognition accuracy is not so high, it is considered that using them as one of the segmentation hints is sufficiently effective enough to substitute for user input. It should be noted that even if the user inputs information using a mouse, it is equivalent in that only very limited information can be obtained. This result of wavelet analysis is used in graph-cuts-based BMC segmentation.

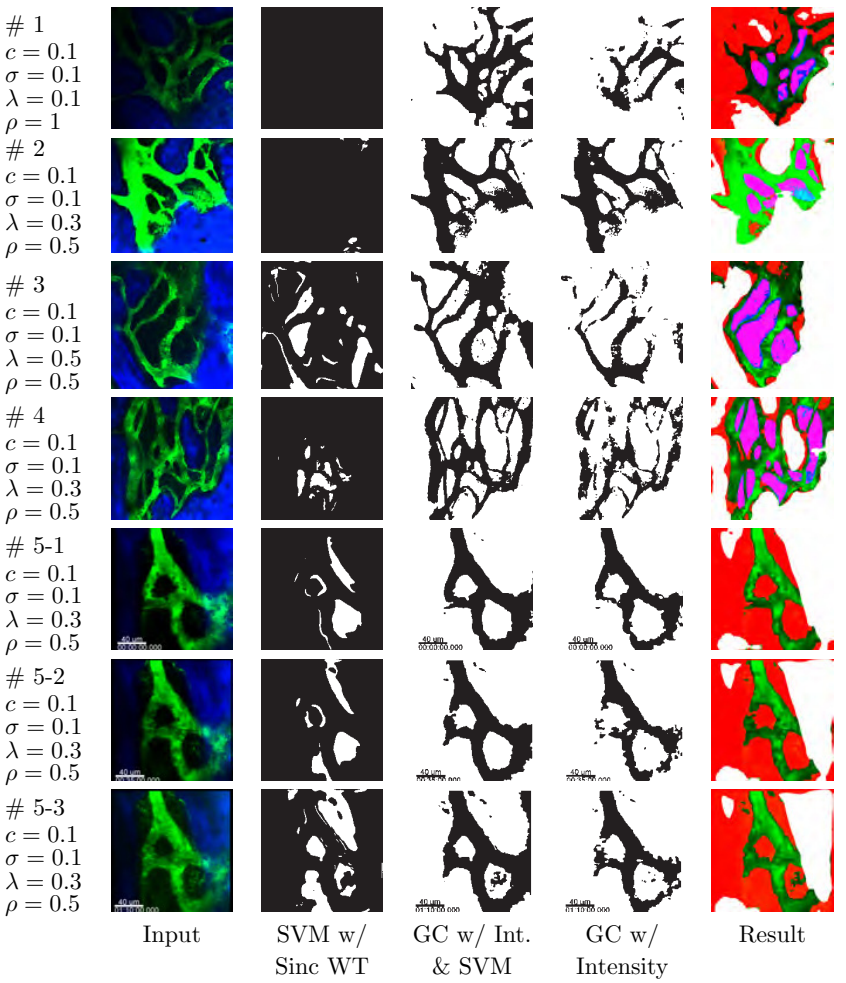

Fig. 6. Examples of the results: Regarding the images of Nos. 1–4, the classifier is trained from all datasets except itself. Regarding the images of No. 5, there are no ground truths, and the classifier is trained from dataset Nos. 1–4. The first column shows image No. and parameters for energy function. The second column shows input images (the first frame of each dataset), where each channel shows the same as Fig. 4. The third column shows the results of classification with SVM and Sinc WT. The fourth column shows the results of graph-cuts with proposed energy function consisting of intensity and classification with SVM and Sinc WT. The fifth column shows the results of graph-cuts with intensity. The sixth column shows superposition as a result of bone segmentation, a result of proposed graph-cuts, and the ground truth, where green shows regions segmented as blood vessel, red shows regions segmented as BMC, blue shows the ground truth of BMC, and white shows the regions segmented as bone. Thus, magenta pixels mean true positive.

4.2. *BMC segmentation*

The results of BMC segmentation by graph-cuts are shown in the "Result" column in Fig. 6. As mentioned in Sec. 4.1, cross-validation is conducted: three datasets are used for SVM training, remaining one is for testing. In segmentation, we used

Table 4. Comparison with intensity based segmentation.

Dataset	Method	Precision	Recall	F-measure
1	Intensity	0.129	0.947	0.227
1	Proposed	0.123	0.725	0.219
2	Intensity	0.470	0.860	0.608
2	Proposed	0.496	0.807	0.615
3	Intensity	0.493	0.974	0.655
3	Proposed	0.681	0.830	0.745
4	Intensity	0.507	0.948	0.660
4	Proposed	0.631	0.861	0.728

the binary image generated from SVM classifiers trained from all datasets except itself. For example, the second column of Image No. 1 in Fig. 6 is generated using classifiers trained from Image Nos. 2, 3, and 4, and then this image is used for the graph-cuts input. Bone regions are excluded from evaluation by segmenting with a simple method: Gaussian smoothing and thresholding. As the result of searching parameters manually, the standard deviation of the Gaussian filter is set to 30, the filter size 30×30, and threshold 0.2. Table 4 shows the quantitative comparison between the proposed method and intensity-based graph-cuts (namely $\lambda = 0$ in Eqs. (4) and (5).

In Image No. 1, the BMC regions cannot be obtained. Possible causes include too low intensity across the image sequence. Regarding Image No. 2, there are also many false negative pixels. However, in this case, pixel-based segmentation performs well. Regarding Image Nos. 3 and 4, the proposed segmentation method is better than that even though the intensity-based graph-cuts performs well. Moreover, while the low intensity areas in the blood vessel region are not correctly segmented with the intensity-based graph-cuts, our method tends to correctly segment continuous blood vessel region. As shown in Table 4, precision improves overall while recall reduces. Since precision and recall are in a trade-off relationship, F-measure is introduced for evaluation, and the F-measures are totally improved in the proposed method. In the case of Image Nos. 3 and 4, the BMC regions seem to be segmented correctly and quantitative evaluation also reflects that. Even if the texture classification fails, the segmentation result is not extremely worse. This result indicates that the wavelet-based texture feature is effective for BMC segmentation, and the proposed method essentially improves the segmentation results without many manual inputs for each image or dataset by a user.

Image Nos. 5-1–5-3 are additional examples of a continuous sequence that FITC seeps out from blood vessels. Although there is no ground truth in this sequence, basically the blood vessel region is the green area in Image No. 5-1. In this experiment, the classifier of texture pattern is generated using all datasets Nos. 1–4. In case the intensity-based segmentation is applied to this sequence, the segmented blood

vessels are not correctly segmented in some low intensity areas. However, some of them are recovered using our method.

The trend similar to Image No. 5 is found in some other image sequences. Moreover, although some high intensity areas in BMC regions are possibly segmented as blood vessels with the intensity-based method, they are essentially segmented as the correct region with the proposed method.

5. Conclusion

In this paper, we presented a BMC segmentation method for an image using multiphoton excitation microscopy. To reduce the need for manual inputs by a user, we applied BMC classification based on wavelet-based texture analysis. We also integrated the result of texture pattern classification into the graph-cuts-based segmentation method to consider spatial continuity. In the experiment, we evaluated various types of mother wavelets and sets of scale parameters, and confirmed that Sinc wavelet and the base scale parameter set $\{2, 4, 16, 32, 64\}$ works better than others. The comparison with intensity-based graph-cuts demonstrates that our method essentially improves BMC segmentation. Even if texture classification fails, the segmentation result is not extremely worse. Future work includes an automated adjustment of the parameters and automated preprocessing of input images. Also, deep learning has been widely used these days. In order to apply deep learning to our research, the amount of data is considered to be insufficient. It is necessary to study methods that work well with less data such as data augmentation.

Acknowledgments

This work was supported by JST CREST Grant No. JPMJCR15G1, Japan, the HPCI System Research project (Project ID:hp170265), and JSPS KAKENHI Grant No. JP16K125250.

References

1. Kikuta J, Wada Y, Kowada T, Wang Z, Sun-Wada G, Nishiyama I, Mizukami S, Maiya N, Yasuda H, Kumanogoh A, Kikuchi K, Germain RN, Ishii M, Dynamic visualization of RANKL and Th17-mediated osteoclast function, *J Clin Invest* **123**:866–873, 2013.
2. Mashita T, Usami J, Shigeta H, Kuroda Y, Kikuta J, Senoo S, Ishii M, Matsuda H, Takemura H, A segmentation method for bone marrow cavity image using graph-cuts, *1st Workshop on Pattern Recognition Techniques for Indirect Immunofluorescence Images*, pp. 20–23, 2014.
3. Shigeta H, Mashita T, Kikuta J, Seno S, Takemura H, Matsuda H, Ishii M, A graph cuts image segmentation method for quantifying barrier permeation in bone tissue, *1st Workshop on Pattern Recognition Techniques for Indirect Immunofluorescence Images*, pp. 16–19, 2014.

4. Shigeta H, Mashita T, Kaneko T, Kikuta J, Senoo S, Takemura H, Matsuda H, Ishii M, A bone marrow cavity segmentation method using wavelet-based texture feature, *23rd Int Conf Pattern Recognition (ICPR)*, No. TuPT5.3, 2016.
5. Fujisaki K, Hamano A, Aoki K, Feng Y, Uchida S, Araseki M, Saito Y, Suzuki T, Detection and tracking protein molecules in fluorescence microscopic video, *The 1st Int Workshop on BioImage Recognition*, pp. 270–274, 2013.
6. Meijering E, Dzyubachyk O, Smal I, Van Cappellen WA, Tracking in cell and developmental biology, *Semin Cell Dev Biol* **20**:894–902, 2009.
7. Liu AA, Li K, Kanade, T, Mitosis sequence detection using hidden conditional random fields, *IEEE Int Symp Biomedical Imaging: From Nano to Macro*, pp. 580–583, 2010.
8. Olivieri D, Faro J, Gomez-Conde I, Tadokoro CE, Tracking T and B cells from two-photon microscopy imaging using constrained SMC clusters, *J Integr Bioinform* **8**:180, 2011.
9. Garvin MK, Abràmoff MD, Kardon R, Russell SR, Wu X, Sonka M, Intraretinal layer segmentation of macular optical coherence tomography images using optimal 3D graph search, *IEEE Trans Med Imag* **27**:1495–1505, 2008.
10. Danesh H, Kafieh R, Rabbani H, Hajizadeh F, Segmentation of choroidal boundary in enhanced depth imaging OCTs using a multiresolution texture based modeling in graph cuts, *Comput Math Methods Med*, 479268, 2014.
11. Yin Z, Li K, Kanade T, Chen M, Understanding the optics to aid microscopy image segmentation, *Int Conf Medical Image Computing and Computer-Assisted Intervention*, pp. 209–217, 2010.
12. Lagarias JC, Reeds JA, Wright MH, Wright PE, Convergence properties of the Nelder–Mead simplex method in low dimensions, *SIAM J Optim* **9**:112–147, 1998.
13. Boykov Y, Jolly MP, Interactive graph cuts for optimal boundary & region segmentation of objects in ND Images, *Int Conf Comput Vis* pp. 105–112, 2001.
14. Boykov Y, Funka-Lea G, Graph cuts and efficient nd image segmentation, *Int J Comput Vis*, **70**:109–131, 2006.
15. Boykov Y, Kolmogorov V, maxflow, Available at http://pub.ist.ac.at/~vnk/software.html, Last Accessed 28, April 2017.
16. Collins TJ, ImageJ for microscopy, *Biotechniques* **43**:25–30, 2007.
17. Biomedical Imaging Group: TurboReg. Available at http://bigwww.epfl.ch/thevenaz/turboreg/. Last accessed 28, April 2017.
18. Biomedical Imaging Group: StackReg. Available at http://bigwww.epfl.ch/thevenaz/stackreg/. Last accessed 28, April 2017.
19. Torrence C, Compo GP, A practical guide to wavelet analysis, *Bull Am Meteorol Soc* **79**:61–78, 1998.

Hironori Shigeta is a Specially Appointed Assistant Professor (CREST, JST) of the Graduate School of Information Science and Technology, Osaka University. He received his B.E., M.E., and Ph.D. degrees from Osaka University in 2008, 2010, and 2016, respectively. He is a member of IPSJ, VRSJ, and ACM.

Tomohiro Mashita graduated from Osaka University in 2001 and completed the M.S. and doctoral programs in 2003 and 2006, respectively. He was a postdoctoral fellow at Osaka University from 2006 to 2008. He was a senior research fellow at Graz University of Technology from 2012 to 2013. He is currently an Associate Professor at Cybermedia Center, Osaka University. His research interest includes Computer Vision, and Pattern Recognition. He is a member of the IEICE, IPSJ, VRSJ, and IEEE.

Junichi Kikuta, M.D., Ph.D. is an Assistant Professor in the Department of Immunology and Cell Biology, Graduate School of Medicine, Osaka University. He was graduated from the Osaka University Medical School in 2006, and then worked as a rheumatologist. He received his Ph.D. degree in 2013. His research interests include intravital imaging of the immune system and bone metabolism.

Shigeto Seno is an Assistant Professor of the Graduate School of Information Science and Technology, Osaka University. He received his B.E., M.E., and Ph.D. degrees from Osaka University in 2001, 2003, and 2006, respectively. He is a member of IPSJ, JSBi, and MII.

Haruo Takemura received his BE, ME, and PhD degrees from Osaka University in 1982, 1984, and 1987, respectively. In 1987, he joined Advanced Telecommunication Research Institute, International. In 1994, he joined Nara Institute of Science and Technology, as an Associate Professor in the Graduate School of Information Science and Technology. From 1998 to 1999, he was a visiting Associate Professor at the University of Toronto, Ontario, Canada. He is a Professor at Cybermedia Center, Osaka University since 2001. His research interests include interactive computer graphics, human–computer interaction, and mixed reality. He is a member of the IEICE, the IPSJ, the VRSJ, the HIS, the IEEE, and the ACM.

Masaru Ishii, M.D., Ph.D. (Professor of Immunology and Cell Biology, Graduate School of Medicine and Frontier Biosciences, Osaka University) was graduated from the Osaka University Medical School in 1998, and then worked as a Physician specialized in rheumatology and internal medicine. He studied in the National Institutes of Health as a research fellow supported by the Human Frontier Science Program (2006–2008), as a Laboratory Chief in Osaka University Immunology Frontier Research Center (Associate Professor; 2008–2011, Professor; 2011–2013), and then appointed as a Professor and Chairman of the Department of Immunology and Cell Biology, Graduate School of Medicine, Osaka University, since 2013. The bulk of his studies has so far elucidated the cellular dynamics in live bone tissues, with a special focus on bone-resorbing osteoclasts, by using intravital multiphoton-based bone imaging that he has originally developed. His study is not limited in the field of bone biology, but is currently covering diverse research topics where cells are dynamically moving, such as immune cell migration in inflammatory sites and cancer invasion/metastases.

Hideo Matsuda received his B.Sc. degree in Physics from Kobe University, Japan, in 1982, and he received his M.E. and Ph.D. degrees in Computer Science from Kobe University, Japan, in 1984 and 1987, respectively. He has been a Professor in the Department of Bioinformatic Engineering, Graduate School of Information Science and Technology, Osaka University, since 2002. His research interests include genomic data analysis, gene regulatory networks, and gene expression analysis.